

Chemical Science

Volume 16
Number 32
28 August 2025
Pages 14411-14824

rsc.li/chemical-science



ISSN 2041-6539

EDGE ARTICLE

Ming Liu *et al.*

Construction of helicates based on six-coordinated silicon centres

Cite this: *Chem. Sci.*, 2025, 16, 14448

All publication charges for this article have been paid for by the Royal Society of Chemistry

Received 6th May 2025
Accepted 14th July 2025

DOI: 10.1039/d5sc03271g

rsc.li/chemical-science

Construction of helicates based on six-coordinated silicon centres†

Yu-Tao Guan,^a Heng Ji,^a Ju Yang,^a Sai-Sai Yu^a and Ming Liu^{ID}*^{ab}

A class of triple-stranded helicates based on six-coordinate silicon centres has been constructed through self-assembly of achiral catechol ligands, as confirmed by single-crystal X-ray diffraction. These architectures demonstrate stability across physiological environments at pH = 3–12. Ligand rigidity dictates chiral configurations: rigid scaffolds form $\Delta\Delta/\Delta\Delta$ racemic helicates, while flexible linkers enable dynamic equilibration with $\Delta\Delta$ mesostates, observable by NMR. Host–guest interactions drive mesocate to helicate conversion, imparting cage-like guest recognition behavior. The helicates combine the biocompatibility of silicon with ligand-controlled chirality switching, offering potential for biomimetic applications.

Introduction

Supramolecular self-assembly, governed by non-covalent interactions, serves as the fundamental driving force for the formation of numerous ordered architectures in nature. Notably, naturally occurring helical motifs, such as the DNA double helix and the collagen triple helix, are ubiquitously distributed across biological systems and play pivotal roles in vital life processes.¹ Inspired by these natural helices, which exhibit an exquisite integration of structural elegance and functional significance, extensive research efforts have been devoted to the rational design and synthesis of artificial helical architectures, particularly supramolecular helices with highly tunable properties, to develop biomimetic analogs with advanced functionalities. Conventionally, the construction of supramolecular chiral assemblies relies on chiral building blocks, whereas achieving well-defined chiral nanostructures from entirely achiral molecular motifs remains a significant challenge in the field.²

Metal–ligand self-assembly enables the construction of complex architectures from simple organic ligands. Through dynamic and pre-designed coordination interactions, a diverse array of supramolecular structures, including metal–organic cages (MOCs), coordination polymers (CPs), metal–organic frameworks (MOFs), molecular knots, *etc.*, have been successfully assembled.³ Among these, one of the most fundamental motifs is the triple helix structure, which consists of two octahedral metal centres bridged by organic ligands.⁴ In 1987, Lehn *et al.* introduced the term “helicate” to describe such metal-

coordinated self-assembled structures.⁵ In fact, helicates can essentially be viewed as simplified coordination cages. Nevertheless, such unique “coordination cages” seldom exhibit host–guest complexation capabilities due to their limited cavity size.⁶ Recent developments have successfully extended their construction to incorporate numerous metal ions including Ga³⁺, Fe²⁺, Ti⁴⁺, Zn²⁺, *etc.*, for the formation of helical structures.⁷ Recently, Zhang *et al.* successfully constructed helical polymers ranging from self-organized to mechanically entangled architectures through supramolecular interactions between achiral tetracoordinate borate complexes.⁸ Despite these advances, metal-centered triple helicates often exhibit limited biocompatibility, which restricts their applicability in biological systems. To address this challenge, the development of helicates with biocompatible coordination centres—instead of heavy metals—represents a promising strategy for constructing highly biomimetic helical structures with enhanced biological relevance.

Silicate materials have garnered significant attention in tissue engineering and regenerative medicine due to their unique “bioactive-degradable-multifunctional” triad of properties.⁹ While silicon typically exists in four-coordinate configurations in silicate systems, recent work by Jiang *et al.* has expanded this paradigm by demonstrating that silicon can also adopt planar quadrilateral geometries in covalent organic frameworks (COFs) through strategic d-orbital hybridization.^{10e} Nevertheless, the presence of accessible d-orbitals enables the formation of higher coordination states (five- or six-coordinate species), though such structures generally require stabilization by highly electronegative elements (F, O, and N), as exemplified by the classic SiF₆²⁻. The dynamic character of Si–O bonds has more recently facilitated their incorporation into COFs,¹⁰ coordination polymers¹¹ and coordination organic cages.¹² Despite these advances, the construction of triple-

^aDepartment of Chemistry, Zhejiang University, Hangzhou, 310058, China^bHangzhou Global Scientific and Technological Innovation Center (HIC), Zhejiang University, Xiaoshan, Hangzhou 311215, China. E-mail: mingliu@zju.edu.cn† Electronic supplementary information (ESI) available. CCDC 2447708–2447714. For ESI and crystallographic data in CIF or other electronic format see DOI: <https://doi.org/10.1039/d5sc03271g>



Scheme 1 (a) Representative Si–O coordination modes used in the construction of supramolecular structures in previous studies. (b) Construction of chiral helices by achiral ligands based on six-coordinated $[\text{SiO}_6]^{2-}$. (c) Single-crystal structures of five helicates with different catechols (the distance between two $[\text{SiO}_6]^{2-}$ centres in the single-crystal structure was measured).

stranded helices centered on six-coordinate silicon remains unexplored.

Herein, we have developed a class of helical architectures based on six-coordinate silicon centres, with single-crystal XRD analysis unambiguously confirming the formation of these six-coordinate species, which exhibit acid–base stability in physiological environments (Scheme 1b). Systematic investigations reveal that structural control can be achieved through judicious ligand design: branched rigid ligands afford $\Lambda\Lambda/\Delta\Delta$ racemic mixtures, ligands with defined dihedral angles yield an additional $\Lambda\Delta$ mesocate, and flexible ligands enable dynamic interconversion from $\Lambda\Lambda/\Delta\Delta$ to $\Lambda\Delta$ states observable on the NMR timescale. The incorporation of suitable guest molecules induces conformational adaptation, driving the transformation from $\Lambda\Delta$ to $\Lambda\Lambda/\Delta\Delta$ (Scheme 1a).

Results and discussion

Catechol was chosen as an ideal ligand for reaction with $\text{Si}(\text{OMe})_4$ due to its distinctive diphenol chelate structure. For instance, the diamine ligand N,N' -([1,1'-biphenyl]-4,4'-diyl) bis(2,3-dihydroxybenzamide) (H_4B) was synthesized through amide condensation between p -phenylenediamine (NH_2B) and 2,3-dimethoxybenzoyl chloride in DCM solvent with Et_3N as the acid scavenger, yielding Me_4B in 82%. Subsequent demethylation of Me_4B using BBr_3 produced H_4B in 87% yield. All other

catechol ligands were synthesized following identical reaction conditions (Fig. S1, ESI†).

The reaction of H_4B , MeONa , and $\text{Si}(\text{OMe})_4$ in a stoichiometric ratio of 3 : 4 : 2 in methanol at room temperature for 4 days yielded the triple-stranded helicate $\text{Na}_4[\text{Si}_2\text{B}_3]$ in 75.8% yield (Fig. 1a and b). Under identical conditions, $\text{Na}_4[\text{Si}_2\text{A}_3]$ was similarly obtained. As illustrated in Fig. 2a, the conversion of H_4B to the helicate $\text{Na}_4[\text{Si}_2\text{B}_3]$ was accompanied by significant upfield shifts of the aromatic protons. Notably, the amide proton H_f exhibited a substantial downfield shift from 10.4 to 12.0 ppm, attributed to the formation of a stronger intramolecular hydrogen bond with the deprotonated phenolic hydroxyl group. Diffusion-ordered ^1H NMR spectroscopy (DOSY) experiments not only confirmed the presence of discrete species but also provided crucial diffusion coefficient data, serving as evidence for the subsequent formation of chiral isomers (Fig. 1c and Table 1). The ^{29}Si NMR spectrum displayed a characteristic singlet at -141.1 ppm (Fig. S18, ESI†), a chemical shift significantly upfield compared to those of tetrahedral $\text{Si}(\text{OMe})_4$ (-35 to -50 ppm) and the planar quadrilateral SiO_4 moieties in reported COFs (-100 ppm), further confirming the unique electronic environment of the six-coordinate silicon species.^{10e} ESI-MS analysis of $\text{Na}_4[\text{Si}_2\text{B}_3]$ in methanol revealed charge-state distributions from 3^- to 1^- for the $[2 + 3]$ helicate assembly (Fig. S35–S38, ESI†), providing additional confirmation of the helical structure formation.





Fig. 1 (a) Schematic diagram of synthesizing $\text{Na}_4[\text{Si}_2\text{L}_3]$ from H_4L (L = A–E). (b) Comparison of ^1H NMR spectra (600 MHz, $\text{DMSO}-d_6$, and 298 K) of H_4B and $\text{Na}_4[\text{Si}_2\text{B}_3]$. (c and d) Diffusion-ordered ^1H NMR spectroscopy (DOSY) spectra (500 MHz, $\text{DMSO}-d_6$, and 298 K) of $\text{Na}_4[\text{Si}_2\text{B}_3]$ and $\text{Na}_4[\text{Si}_2\text{D}_3]$ (* represents helicates ($\Delta\Delta/\Delta\Delta$)).



Fig. 2 ^1H NMR spectrum (600 MHz, $\text{DMSO}-d_6$, 298 K) of the transformation of $\text{Na}_4[\text{Si}_2\text{D}_3]$ from helicates ($\Delta\Delta/\Delta\Delta$) to mesocate ($\Delta\Delta$) over time. (▲) represents helicates ($\Delta\Delta/\Delta\Delta$) and * represents mesocate ($\Delta\Delta$).

In contrast to other derivatives, the reactions of $\text{Na}_4[\text{Si}_2\text{C}_3]$, $\text{Na}_4[\text{Si}_2\text{D}_3]$ and $\text{Na}_4[\text{Si}_2\text{E}_3]$ required 80 °C to proceed efficiently, likely due to the presence of ligand dihedral angles that facilitate oligomer formation, and therefore elevated reaction

Table 1 Hydrodynamic radii calculated from DOSY results

	$\lg D$ ($\lg \text{cm}^2 \text{s}^{-1}$)	D ($10^{-7} \text{cm}^2 \text{s}^{-1}$)	r^a (Å)
$\text{Na}_4[\text{Si}_2\text{A}_3]$	−6.055	8.810	12.41
$\text{Na}_4[\text{Si}_2\text{B}_3]$	−6.128	7.447	14.69
$\text{Na}_4[\text{Si}_2\text{C}_3]$	−6.130	7.413	14.76
$\text{Na}_4[\text{Si}_2\text{D}_3]$	−6.068	8.551	12.79
$\text{Na}_4[\text{Si}_2\text{E}_3]$	−6.067	8.570	12.77

^a The hydrodynamic radii (r) of the indicated helicates were calculated by using the Stokes–Einstein equation $r = kT/6\pi\eta D$, where k is the Boltzmann constant ($1.3807 \times 10^{-23} \text{m}^2 \text{kg s}^{-2} \text{K}^{-1}$), T is the temperature in Kelvin, η is the viscosity of the solution ($1.19 \times 10^{-3} \text{kg m}^{-1} \text{s}^{-1}$ for DMSO), and D is the diffusion coefficient.

temperatures are needed to accelerate the Si–O dynamic reversible process (Fig. S27, ESI[†]). ^1H NMR spectroscopy revealed distinct structural behaviors among the complexes. While $\text{Na}_4[\text{Si}_2\text{A}_3]$ and $\text{Na}_4[\text{Si}_2\text{B}_3]$ each displayed a single resonance signal, $\text{Na}_4[\text{Si}_2\text{C}_3]$ and $\text{Na}_4[\text{Si}_2\text{D}_3]$ exhibited two discrete signals (Fig. S7–S10, ESI[†]). Notably, these signals gradually equilibrated to a fixed ratio over time, with this phenomenon being particularly pronounced in $\text{Na}_4[\text{Si}_2\text{D}_3]$. In contrast, $\text{Na}_4[\text{Si}_2\text{C}_3]$ showed only minor spectral changes. DOSY spectroscopy confirmed that all species possessed identical diffusion coefficients, effectively excluding the possibility of higher-order assemblies with increased combinatorial complexity (Fig. 1d). The differences in spectra arise from the interplay between the helical chirality at the complexation centres of the helicates and the conformational flexibility of the linkages (H_4C , H_4D , and H_4E). This combination enables dihedral angle modulation, resulting in the coexistence of helicate ($\Delta\Delta/\Delta\Delta$) and mesocate ($\Delta\Delta$) chiral isomers.

Single crystals suitable for X-ray diffraction were successfully obtained through vapor diffusion of diethyl ether into methanol solutions of the five helicates. X-ray crystallographic analysis revealed distinct configuration preferences among these complexes: the spiral chiral centres in $\text{Na}_4[\text{Si}_2\text{A}_3]$ and $\text{Na}_4[\text{Si}_2\text{B}_3]$ exclusively adopted the helicate ($\Delta\Delta/\Delta\Delta$) configuration, consistent with their observation of a single set of signals in the ^1H NMR spectra. In contrast, $\text{Na}_4[\text{Si}_2\text{C}_3]$ and $\text{Na}_4[\text{Si}_2\text{D}_3]$ crystallized in the mesocate ($\Delta\Delta$) configuration, with no evidence of $\Delta\Delta/\Delta\Delta$ conformers observed in the solid state (Fig. 3a). This configurational preference likely stems from the comparable thermodynamic stability of both helicate and mesocate forms, resulting in their coexistence during the synthetic process. Solution-phase studies revealed a gradual conversion from helicate to mesocate configurations over time, with the transformation kinetics being particularly accelerated in $\text{Na}_4[\text{Si}_2\text{D}_3]$. The enhanced conformational flexibility imparted by the ether linkage in this complex facilitated rapid configurational interconversion, as evidenced by the evolution of the ^1H NMR signals from an initial 53 : 47 (mesocate : helicates) ratio to a final equilibrium ratio of 88.5 : 11.5 (Fig. 2). These observations highlight the critical role of ligand flexibility in governing the dynamic equilibrium between different helical configurations. Furthermore, when acetonitrile is employed as the





Fig. 3 (a) Helical chiral configurations of five assemblies as illustrated in the single-crystal structures. (b) The cavity size of the $\text{Na}_4[\text{Si}_2\text{E}_3]$ $\Delta\Delta/\Delta\Delta$ (for structural clarity and precision, the counterion Na^+ and all hydrogens are omitted). (c and d) The SC-XRD diffraction packing pattern of $\text{Na}_4[\text{Si}_2\text{C}_3]$ single crystal obtained in acetonitrile/diethyl ether.

crystallization solvent, well-ordered layered structures will be obtained. In contrast, methanol exhibits strong solvation effects toward Na^+ , occupying its coordination sites and consequently leading to relatively disordered structures (Fig. 3c and d).

Previous research on Ti-centered helicates has demonstrated that ligands containing an odd number of connecting units preferentially form mesocates due to inherent geometrical constraints.¹³ Surprisingly, the $\text{Na}_4[\text{Si}_2\text{E}_3]$ exhibits an unusual helicate assembly behavior, contradicting conventional ligand structure-directing principles. Upon introduction of excess H_2O and heating at 70°C , we observe near-complete transformation from mesocate to helicate configurations (Fig. 4). Single-crystal X-ray analysis unambiguously confirms the encapsulation of $\text{Na}(\text{H}_2\text{O})_2^+$ units within the helicate cavity, providing direct evidence for host-guest complexation. Comparative structural analysis reveals that while the helicate's spacious cavity readily accommodates the $\text{Na}(\text{H}_2\text{O})_2^+$ guest (Fig. 3b), the more compact mesocate (exemplified by $\text{Na}_4[\text{Si}_2\text{C}_3]$ and $\text{Na}_4[\text{Si}_2\text{D}_3]$) lacks the necessary space. A similar phenomenon has been observed by Raymond *et al.* in the conversion of thermodynamically stable

mesocates into helicates upon interaction with suitable guest molecules.¹⁴ The guest-induced stabilization energy effectively offsets the helicate's intrinsic thermodynamic penalty, illustrating a remarkable example of supramolecular conformational adaptation through dynamic equilibrium control. This consequently endows the helicates with the host-guest recognition capability characteristic of the coordination cage.

The distinctive $[\text{SiO}_6]^{2-}$ structure has prompted examination of its stability characteristics. This six-coordinate silicate structure, while theoretically expected to demonstrate significant pH sensitivity, exhibits remarkable stability when incorporated into the helicates based on six-coordinated silicon centres. Since all five helicates share identical $[\text{SiO}_6]^{2-}$ fragments, we selected $\text{Na}_4[\text{Si}_2\text{B}_3]$ with its singular NMR signature as the representative system for investigation. The anionic nature of this compound enables aqueous solubility at physiological temperature (37°C), with ^1H NMR analysis confirming structural integrity after 24 hours in solution. This stability stands in stark contrast to $[\text{SiO}_6]^{2-}$ -containing COFs,^{9a} which undergo structural degradation upon suspending in water or



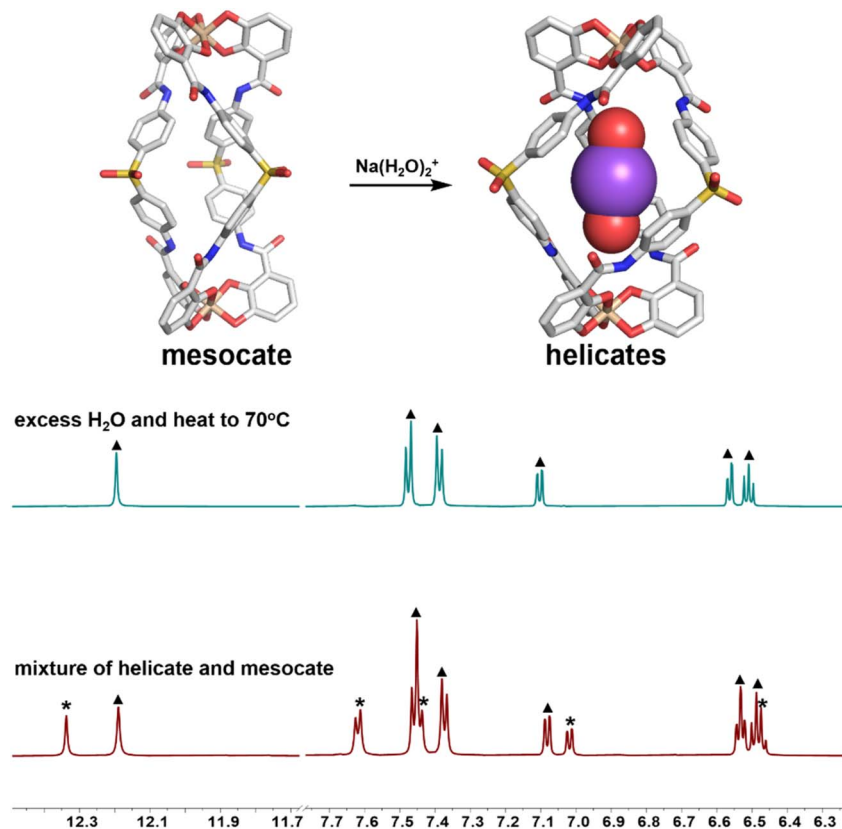


Fig. 4 Comparison of ^1H NMR spectra (600 MHz, $\text{DMSO}-d_6$, and 298 K) of mixtures of $\text{Na}_4[\text{Si}_2\text{E}_3]$ isomers before and after heating with excess H_2O at 70°C . (\blacktriangle represents helicates ($\Delta\Delta/\Delta\Delta$) and $*$ represents mesocate ($\Delta\Delta$)).

under humid conditions. The exceptional stability of $\text{Na}_4[\text{Si}_2\text{B}_3]$ could be attributed to stabilizing triple hydrogen bonds between the catechol ligand's N-H and the $[\text{SiO}_6]^{2-}$ segment. Remarkably, the strongly alkali conditions employed in $\text{Na}_4[\text{Si}_2\text{B}_3]$ synthesis presage its alkali stability, with the

structure demonstrating complete integrity even at $\text{pH} = 12$. Further stability testing revealed that the helical architecture remains essentially unchanged after 24 hours of exposure to weakly acidic conditions ($\text{pH} = 3-4$). Structural decomposition to the free H_4B ligand occurs only when the pH is reduced to 2



Fig. 5 ^1H NMR spectrum (600 MHz, $\text{DMSO}-d_6$, and 298 K) of $\text{Na}_4[\text{Si}_2\text{B}_3]$ in aqueous solutions at $\text{pH} = 2, 3, 4, 7,$ and 12 , respectively.



(Fig. 5). The demonstrated pH stability range (pH = 3–12) encompasses nearly all physiological environments within the human body, while enabling selective decomposition and sustained drug release under highly acidic conditions, such as those found in gastric compartments or acid-exposed lesions. Additionally, the other four helicates demonstrate the same excellent stability (Fig. S28†). Such characteristics position these highly coordinated silicon-based helical structures as promising candidates for biomedical applications, such as in targeted drug delivery systems and biosensor development, where pH stability across physiological ranges represents a critical requirement.

Conclusions

In summary, we have developed a category of supramolecular helicates based on six-coordinate silicon centres, which exhibit acid–base stability in physiological environments. A well-defined three-stranded helicate system was established through the controlled self-assembly of rationally designed catechol-derived ligands with Si(OMe)₄. Single-crystal X-ray diffraction analysis unambiguously confirms the formation of [SiO₆]^{2−} coordination cores and elucidates the critical structure-directing role of ligand design: rigid ligands exclusively yield $\Lambda\Lambda/\Delta\Delta$ racemic helicates, while flexible ligands enable dynamic equilibration between helicate ($\Lambda\Lambda/\Delta\Delta$) and mesocate ($\Lambda\Delta$) conformations, as directly monitored by NMR spectroscopy. Remarkably, we demonstrate that host–guest interactions can override thermodynamic preferences, as evidenced by the Na(H₂O)₂⁺ encapsulation-induced stabilization of otherwise disfavored helicate configurations. This study expands the repertoire of coordination centres available for supramolecular helicates while addressing the biocompatibility limitations of conventional metal-based systems. More importantly, this work establishes a ligand engineering approach for precise control over helical dynamics, opening new avenues for designing biomimetic architectures.

Data availability

The data supporting this article have been included as part of the ESI† Crystallographic data (for compounds Na₄[Si₂A₃], Na₄[Si₂B₃], Na₄[Si₂C₃], Na₄[Si₂D₃] and Na₄[Si₂E₃]) have been deposited at the CCDC under CCDC number (2447708–2447714) and can be obtained from <https://www.ccdc.cam.ac.uk/>.

Author contributions

Yu-Tao Guan: project design, synthesis, characterization, data analysis, and article writing. Heng Ji: crystal structure analysis. Ju Yang: theoretical guidance. Sai-Sai Yu: diagram preparation. Ming Liu: project design, theoretical direction, funding acquisition, project administration, resources, supervision, and writing – review & editing.

Conflicts of interest

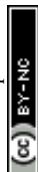
There are no conflicts to declare.

Acknowledgements

The authors gratefully acknowledge the National Natural Science Foundation of China (no. 22371252), the Zhejiang Provincial Natural Science Fund (LZ23B020005), and the Leading Innovation Team grant from the Department of Science and Technology of Zhejiang Province (2022R01005). The authors also thanks the Roentgen Laboratory for XRD testing and technical support.

Notes and references

- (a) P. Zhan, A. Peil, Q. Jiang, D. Wang, S. Mousavi, Q. Xiong, Q. Shen, Y. Shang, B. Ding, C. Lin, Y. Ke and N. Liu, *Chem. Rev.*, 2023, **123**, 3976–4050; (b) L. N. Green, H. K. K. Subramanian, V. Mardanolou, J. Kim, R. F. Hariadi and E. Franco, *Nat. Chem.*, 2019, **11**, 510–520; (c) I. C. Tanrikulu, A. Forticaux, S. Jin and R. T. Raines, *Nat. Chem.*, 2016, **8**, 1008–1014.
- (a) X. Zha, G. Xu, N. A. Khan, Z. Yan, M. Zuo, Y. Xiong, Y. Liu, H. You, Y. Wu, K. Liu, M. Li and D. Wang, *Angew. Chem., Int. Ed.*, 2024, **63**, e202316385; (b) Q. Song, J. Yang, K. Zheng, T. Zhang, C. Yuan, L.-M. Yuan and X. Hou, *J. Am. Chem. Soc.*, 2024, **146**, 7594–7604; (c) J. Zhang, K. Wu, X. Gao, M. Zhang, X. Zhou, F. Bertram, C. Shen and Y. Zhou, *Sci. Adv.*, 2024, **10**, eado5948; (d) D. Wu, K. Zhou, J. Tian, C. Liu, J. Tian, F. Jiang, D. Yuan, J. Zhang, Q. Chen and M. Hong, *Angew. Chem., Int. Ed.*, 2021, **60**, 3087–3094; (e) Y. Li, C. Liu, X. Bai, F. Tian, G. Hu and J. Sun, *Angew. Chem., Int. Ed.*, 2020, **59**, 3486–3490; (f) X. Lou, K. Zhang, Y. Bai, S. Zhang, Y. Li and Y. Yang, *Angew. Chem., Int. Ed.*, 2025, **64**, e202414611.
- (a) H.-N. Zhang and G.-X. Jin, *Angew. Chem., Int. Ed.*, 2023, **62**, e202313605; (b) Q. Zhou, X. Dong, G. Chi, X.-Y. Cao, N. Zhang, S. Wu, Y. Ma, Z.-H. Zhang and L. Zhang, *J. Am. Chem. Soc.*, 2024, **146**, 22405–22412; (c) H. Xu, T. K. Ronson, A. W. Heard, P. C. P. Teeuwen, L. Schneider, P. Pracht, J. D. Thoburn, D. J. Wales and J. R. Nitschke, *Nat. Chem.*, 2025, **17**, 289–296; (d) J. Ruan, Y.-L. Lu, P. Hu and C.-Y. Su, *J. Am. Chem. Soc.*, 2025, **147**, 10475–10484; (e) S. Wu, X. Huang, S. Fu, Z. Li, S. Yin, W. Liao, M. Wang, Y. Lu, M. Bonn, Y. Sun, X. Feng and W. Xu, *Angew. Chem., Int. Ed.*, 2025, **64**, e202419865; (f) Y. Yang, C. Zhang, C. Zhang, Y. Shi, J. Li, B. Johannessen, Y. Liang, S. Zhang, Q. Song, H. Zhang, J. Huang, J. Ke, L. Zhang, Q. Song, J. Zeng, Y. Zhang, Z. Geng, P.-S. Wang, Z. Wang, J. Zeng and F. Li, *Nat. Commun.*, 2024, **15**, 6316; (g) Y.-X. Tan, J. Lin, Q.-H. Li, L. Li, R. A. Borse, W. Lu, Y. Wang and D. Yuan, *Angew. Chem., Int. Ed.*, 2023, **62**, e202302882; (h) L. Shi, Z. Xiong, H. Wang, H. Cao and Z. Chen, *Chem*, 2024, **10**, 2464–2472.
- (a) J. Jiao, J. Dong, Y. Li and Y. Cui, *Angew. Chem., Int. Ed.*, 2021, **60**, 16568–16575; (b) J. Zhu, X.-W. Sun, X. Yang,



- S.-N. Yu, L. Liang, Y.-Z. Chen, X. Zheng, M. Yu, L. Yan, J. Tang, W. Zhao, X.-J. Yang and B. Wu, *Angew. Chem., Int. Ed.*, 2023, **62**, e202314510; (c) R. Chen, Q.-Q. Yan, S.-J. Hu, X.-Q. Guo, L.-X. Cai, D.-N. Yan, L.-P. Zhou and Q.-F. Sun, *Org. Chem. Front.*, 2021, **8**, 2576–2582.
- 5 J. M. Lehn, A. Rigault, J. Siegel, J. Harrowfield, B. Chevrier and D. Moras, *Proc. Natl. Acad. Sci. U. S. A.*, 1987, **84**, 2565–2569.
- 6 (a) T. Haino, H. Shio, R. Takano and Y. Fukazawa, *Chem. Commun.*, 2009, **18**, 2481–2483; (b) Y. Yamasaki, H. Shio, T. Amimoto, R. Sekiya and T. Haino, *Chem.–Eur. J.*, 2018, **24**, 8558–8568; (c) X.-S. Du, Y. Han and C.-F. Chen, *Chem. Commun.*, 2022, **58**, 1326–1329.
- 7 (a) K. J. Howard-Smith, A. R. Craze, H. Zenno, J. Yagyu, S. Hayami and F. Li, *Chem. Commun.*, 2020, **56**, 8838–8841; (b) M. Meyer, B. Kersting, R. E. Powers and K. N. Raymond, *Inorg. Chem.*, 1997, **36**, 5179–5191; (c) C. Mevissen, A. C. N. Kwamen, L. Himmel, X. Chen, M. Brückner, S. Huda, C. Göb, J. Jenniches, I. Oppel, J. S. Ward, K. Rissanen and M. Albrecht, *Eur. J. Org. Chem.*, 2020, **32**, 5161–5172; (d) X. Chen, T. M. Gerger, C. Räuber, G. Raabe, C. Göb, I. M. Oppel and M. Albrecht, *Angew. Chem., Int. Ed.*, 2018, **57**, 11817–11820.
- 8 (a) L. J. Wayment, S. J. Teat, S. Huang, H. Chen and W. Zhang, *Angew. Chem., Int. Ed.*, 2024, **63**, e202403599; (b) Y. Hu, N. Dunlap, H. Long, H. Chen, L. J. Wayment, M. Ortiz, Y. Jin, A. Nijamudheen, J. L. Mendoza-Cortes, S.-h. Lee and W. Zhang, *CCS Chem.*, 2021, **3**, 2762–2770; (c) Y. Hu, S. J. Teat, W. Gong, Z. Zhou, Y. Jin, H. Chen, J. Wu, Y. Cui, T. Jiang, X. Cheng and W. Zhang, *Nat. Chem.*, 2021, **13**, 660–665; (d) Y. Yu, S.-H. Shen, J.-B. Chen, Q.-R. Ding, H.-X. Zhang and J. Zhang, *J. Am. Chem. Soc.*, 2025, **147**, 20770–20777.
- 9 (a) Y. Han, L. Du, J. Wu, H. Zhang, G. Yang, Y. Zheng and C. Wu, *Mater. Today*, 2025, **83**, 64–84; (b) Z. Zhang, C. Fan, Q. Xu, F. Guo, W. Li, Z. Zeng, Y. Xu, J. Yu, H. Ge, C. Yang and J. Chang, *Adv. Sci.*, 2024, **11**, 2407718; (c) W. Ma, Y. Zheng, G. Yang, H. Zhang, M. Lu, H. Ma, C. Wu and H. Lu, *Mater. Horiz.*, 2024, **11**, 2957–2973; (d) P. Sun, Z. Zhang, F. Gao, C. Yang, G. Mang, S. Fu, J. Tian and J. Chang, *Sci. Adv.*, 2025, **11**, eadr7208.
- 10 (a) J. Roeser, D. Prill, M. J. Bojdys, P. Fayon, A. Trewin, A. N. Fitch, M. U. Schmidt and A. Thomas, *Nat. Chem.*, 2017, **9**, 977–982; (b) O. Yahiaoui, A. N. Fitch, F. Hoffmann, M. Fröba, A. Thomas and J. Roeser, *J. Am. Chem. Soc.*, 2018, **140**, 5330–5333; (c) X. Li, Y. Tian, L. Shen, Z. Qu, T. Ma, F. Sun, X. Liu, C. Zhang, J. Shen, X. Li, L. Gao, S. Xiao, T. Liu, Y. Liu and Y. Lu, *Adv. Funct. Mater.*, 2021, **31**, 2009718; (d) C. Li, D.-D. Wang, G. S. H. P. Ho, Z. Zhang, J. Huang, K.-T. Bang, C. Y. Lau, S.-Y. Leu, Y. Wang and Y. Kim, *J. Am. Chem. Soc.*, 2023, **145**, 24603–24614; (e) Z. Liu, W. Liu, Y. Chen, X. Yang, Y. Liu, Y. Jin, Q. Xu, D. Qi, K. Wang, Y. Zhu and J. Jiang, *CCS Chem.*, 2025, **7**, 1812–1822.
- 11 (a) M. Naoe, H. Iwashita, S. Saito, M. Koike, H. Wada, A. Shimojima and K. Kuroda, *Chem. Lett.*, 2020, **49**, 1075–1077; (b) R.-L. Chai, X.-K. Zhang, Z. Zhao, T.-T. Li, G.-Y. Li, J. Zhao, G. Li, B. Cheng, Q. Zhao and S.-H. Li, *ACS Mater. Lett.*, 2023, **5**, 1376–1383.
- 12 (a) J. L. Holmes, B. F. Abrahams, A. Ahveninen, B. A. Boughton, T. A. Hudson, R. Robson and D. Thinnagaran, *Chem. Commun.*, 2018, **54**, 11877–11880; (b) Y. Kawakami, T. Ogishima, T. Kawara, S. Yamauchi, K. Okamoto, S. Nikaido, D. Souma, R.-H. Jin and Y. Kabe, *Chem. Commun.*, 2019, **55**, 6066–6069; (c) C. M. Hong, M. Morimoto, E. A. Kapustin, N. Alzakhem, R. G. Bergman, K. N. Raymond and F. D. Toste, *J. Am. Chem. Soc.*, 2018, **140**, 6591–6595; (d) K. T. Xia, A. Rajan, Y. Surendranath, R. G. Bergman, K. N. Raymond and F. D. Toste, *J. Am. Chem. Soc.*, 2023, **145**, 25463–25470.
- 13 M. Albrecht and S. Kotila, *Angew. Chem., Int. Ed.*, 1995, **34**, 2134–2137.
- 14 J. Xu, T. N. Parac and K. N. Raymond, *Angew. Chem., Int. Ed.*, 1999, **38**, 2878–2882.

